

Energetic cost of microswimmer navigation: The role of body shapeLorenzo Piro ^{1,2} Andrej Vilfan ^{1,3} Ramin Golestanian ^{1,4,*} and Benoît Mahault ^{1,†}¹Max Planck Institute for Dynamics and Self-Organization (MPI-DS), 37077 Göttingen, Germany²Department of Physics & INFN, University of Rome “Tor Vergata”, Via della Ricerca Scientifica 1, 00133 Rome, Italy³Jožef Stefan Institute, 1000 Ljubljana, Slovenia⁴Rudolf Peierls Centre for Theoretical Physics, University of Oxford, Oxford OX1 3PU, United Kingdom

(Received 13 July 2023; accepted 22 February 2024; published 12 March 2024)

We study the energetic efficiency of navigating microswimmers by explicitly taking into account the geometry of their body. We show that, whereas arguments based solely on propulsion efficiency lead one to conclude that needle-like swimmers are most energetically efficient, disk-like swimmers rotated by flow gradients naturally follow time-optimal trajectories. The coupling between body geometry and hydrodynamics thus leads to a generic trade-off between the energetic costs associated with propulsion and navigation, which is accompanied by the selection of a finite optimal aspect ratio. We derive from optimal control theory the steering policy ensuring overall minimum energy dissipation, and characterize how navigation performances vary with the swimmer shape. Our results highlight the important role of the swimmer geometry in realistic navigation scenarios.

DOI: [10.1103/PhysRevResearch.6.013274](https://doi.org/10.1103/PhysRevResearch.6.013274)**I. INTRODUCTION**

Biological microswimmers explore their surroundings in search of food, oxygen, light, mating partners, or to escape predators [1] by means of a variety of swimming mechanisms [2,3]. The energy for propulsion needs to be obtained by exploiting locally available energy sources such as light or nutrients, but their supply is often limited [4]. Bacterial micron-size swimmers such as *E. coli* use their flagella to manipulate the relative significance of translational and rotational friction [5] in order to control their trajectory [6]. Although it has been argued that the metabolic cost of motion is negligible for bacteria [7–9], larger or faster organisms such as *Paramecium* devote a substantial part of their energy turnover to this task [10,11]. In this context, optimizing resources for navigation appears crucial for microswimmers, while it may find application to the design of artificial swimmers [12].

The swimming efficiency of microswimmers can be optimized by designing strategies that minimize the dissipated energy needed to displace the ambient fluid [13–18]. Such optimization problem has been the subject of recent investigation, leading to the statement of minimum dissipation theorems [19,20]. When the swimmer moves in a nonuniform environment, a complementary approach

consists in minimizing the energy dissipated along its trajectory by exploiting the advection provided by the external flow field. Many microswimmers are indeed equipped with receptors that allow them to measure environmental cues such as flow velocity gradient [21], light [22], or chemical concentrations [23], and use this information to navigate [6,24].

As the total energy spent for motion generally grows with the travel time, most theoretical studies on optimal navigation focus on finding time-minimizing trajectories [25–32], with a few exceptions [33,34]. A classical example is the Zermelo problem [35] in which a point-like particle moves at constant speed in a stationary flow field and navigates by adjusting its self-propulsion direction. The corresponding optimal steering policy typically depends on the local flow gradients [25,35]. Real swimmers, on the other hand, have a definite size and shape, and are thus naturally rotated by flow field gradients. Elongated bodies like that of *E. coli*, for instance, undergo Jeffery rotations [36] in shear flows [37–39]. The coupling between flow and swimmer shape is in fact relevant to model encounter rates of microswimmers with moving food sources [40], but its effect on the energy efficiency of navigation remains so far unknown.

In this work, we revisit the problem of optimal navigation taking into account the hydrodynamic implications of the swimmer geometry. We show that, due to a hitherto unnoticed formal relationship between Jeffery rotations and the time-optimal Zermelo steering protocol (ZSP), non-navigating disk-shaped swimmers always follow minimal time trajectories. Considering spheroidal swimmers moving at constant speed, we derive from optimal control theory (OCT) [41] the steering policy that allows them to navigate at minimum energetic cost and discuss how constraints on travel time and energy optimization select a nontrivial optimal swimmer aspect ratio. To highlight the robustness of our findings, we

*ramin.golestanian@ds.mpg.de

†benoit.mahault@ds.mpg.de

Published by the American Physical Society under the terms of the [Creative Commons Attribution 4.0 International license](https://creativecommons.org/licenses/by/4.0/). Further distribution of this work must maintain attribution to the author(s) and the published article's title, journal citation, and DOI. Open access publication funded by the Max Planck Society.

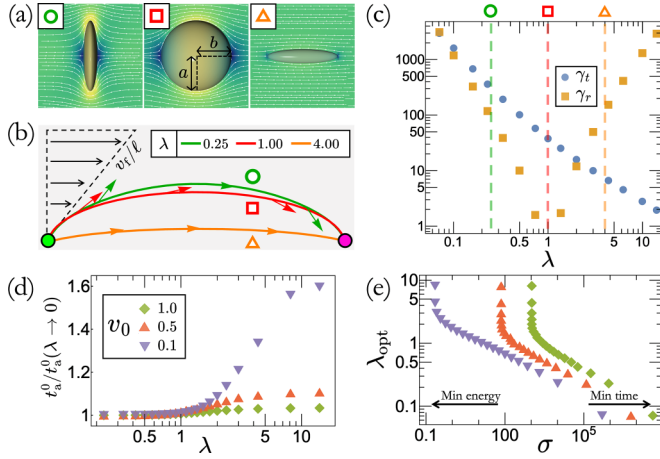


FIG. 1. Smart swimming by “dumb” swimmers. (a) Flow streamlines created by (from left to right) disk-like, spherical, and needle-like swimmers with optimal propulsion [19]. (b) Trajectories of the nonsteering swimmers of the three types shown in panel (a), all starting from \mathbf{r}_0 (green dot) and ending in \mathbf{r}_T (magenta dot). The colored arrows indicate the instantaneous swimming orientation, while the black ones sketch the linear shear flow. (c) The translational and rotational dissipation coefficients obtained from the minimum dissipation theorem [19] as functions of the spheroid aspect ratio λ . (d) Arrival time t_a^0 at the target vs λ normalized by its optimal value at $\lambda \rightarrow 0$ for three different speeds v_0 . (e) Optimal aspect ratio λ_{opt} as function of σ ; legend is the same as (d).

illustrate them in two distinct navigation problems, namely trajectory planning in a linear shear flow and taxis-based navigation in a random flow.

II. OPTIMAL NAVIGATION WITH FINITE-SIZE SWIMMERS

We consider a swimmer moving at constant self-propulsion speed v_0 in the presence of a stationary flow $\mathbf{f}(\mathbf{r})$. We assume this swimmer to be axisymmetric, such that its dynamics is determined by that of its position \mathbf{r} and heading direction $\hat{\mathbf{u}}$ as

$$\dot{\mathbf{r}} = v_0 \hat{\mathbf{u}} + \mathbf{f}(\mathbf{r}), \quad \dot{\hat{\mathbf{u}}} = \boldsymbol{\omega} \times \hat{\mathbf{u}}, \quad (1)$$

where the angular velocity $\boldsymbol{\omega}$ comprises contributions from active torque and passive rotations. Namely, $\boldsymbol{\omega} = \boldsymbol{\omega}_a + \boldsymbol{\omega}_f(\mathbf{r}, \hat{\mathbf{u}})$, where $\boldsymbol{\omega}_a$ is the angular velocity self-generated by the swimmer—hereafter referred to as *the control*—while for axisymmetric bodies in low Reynolds fluids the passive contribution takes the general form $\boldsymbol{\omega}_f(\mathbf{r}, \hat{\mathbf{u}}) \equiv \hat{\mathbf{u}} \times [(\boldsymbol{\Omega} + \boldsymbol{\alpha}\mathbf{S}) \cdot \hat{\mathbf{u}}]$ [36,42]. $\boldsymbol{\Omega}$ is the flow rotation and \mathbf{S} the strain-rate tensor. The coefficient α , known as the *Bretherton constant* [42], is set by the swimmer’s shape. Here, we focus on spheroidal swimmers for which $\alpha = (\lambda^2 - 1)/(\lambda^2 + 1)$ [36], where the aspect ratio $\lambda \equiv b/a$ is defined such that b and a are the dimensions of the spheroid along and transverse to $\hat{\mathbf{u}}$, respectively. As illustrated in Fig. 1(a), $\lambda < 1$ (>1) thus corresponds to disk-like (needle-like) swimmers, while $\lambda = 1$ for spherical swimmers.

In the navigation problems studied below, the initial and target swimmer positions are specified on a given subspace (a point or a line), while its initial and final orientations are

unspecified and determined by the optimization. The efficiency of navigation is measured by the cost,

$$\mathcal{C} \equiv \int_0^{t_a} d\tau [P_{\text{diss}} + \sigma], \quad (2)$$

where t_a is the total travel time. The first contribution to Eq. (2) is the total energy dissipated by the swimmer during navigation, while the parameter σ weights the relative importance of travel time and energy minimization. σ is dimensionally equivalent to a power, and can thus be interpreted as the acceptable power that can be delivered by the swimmer along its trajectory. In general, P_{diss} can be decomposed as the sum of a translational and a rotational component, $P_{\text{diss}} \equiv \mu s [\gamma_t(\lambda) v_0^2 + s^2 \gamma_r(\lambda) |\boldsymbol{\omega}_a|^2]$, where s is a characteristic dimension of the swimmer—here defined as the radius of a sphere with equal volume—and μ denotes the viscosity of the medium. γ_t and γ_r are two dimensionless coefficients that relate the dissipated power to the translational and angular swimming velocities, and take the form of effective drag coefficients. A lower bound on them, corresponding to the data shown in Fig. 1(c) and achieved with theoretically optimal propulsion, is given by the minimum dissipation theorem [19]. This lower bound is expressed in terms of two drag coefficients of bodies with the same shape, one with a no-slip boundary condition and one with a perfect-slip (i.e., no tangential stress), on the surface as $\gamma_i = (R_{\text{PS};i}^{-1} - R_{\text{NS};i}^{-1})^{-1}$ with $i \in \{t, r\}$. For a spheroid with no-slip boundary both translational and rotational drag coefficients are known analytically [43] while for those with perfect-slip boundary we use the numerical results reported in [44]. Here, the aspect ratio λ is varied keeping the swimmer’s volume constant, such that the spheroid dimensions $a = \lambda^{-1/3}s$ and $b = \lambda^{2/3}s$.

III. SMART SWIMMING BY “DUMB” SWIMMERS: THE ROLE OF SHAPE

To investigate how the geometry of a microswimmer’s body alone affects its navigation performance, we first examine the case of a “dumb” swimmer that has no control over its orientation. For now, the active rotation $\boldsymbol{\omega}_a$ is therefore set to $\mathbf{0}$. We consider a two-dimensional linear shear flow $\mathbf{f}(\mathbf{r}) = (v_f y/\ell) \hat{\mathbf{x}}$, where $\mathbf{r} = (x, y)$ and $v_f, \ell > 0$. The point-to-point navigation problem consists in determining the initial orientation $\hat{\mathbf{u}}(0)$ allowing travel between $\mathbf{r}_0 = \mathbf{0}$ and $\mathbf{r}_T = \ell \hat{\mathbf{x}}$. In what follows, we use dimensionless quantities such that lengths, times, and energies are expressed in units of ℓ , ℓ/v_f , and $\mu \ell s v_f$, respectively. In the absence of control, the dimensionless equations of motion (1) depend only on the (dimensionless) swimmer speed v_0 and the aspect ratio λ , such that the arrival time t_a^0 is fully determined by these two parameters. Hence, the cost function (2) reads $\mathcal{C}_0 = t_a^0(v_0, \lambda) [\gamma_t(\lambda) v_0^2 + \sigma]$.

Fixing v_0 , Fig. 1(b) shows that needle-like swimmers ($\lambda > 1$, orange triangle) essentially swim straight to the target and thus remain within weak flow regions. In contrast, disk-like swimmers ($\lambda < 1$, green circle) are more strongly rotated by the shear flow, such that they follow more curved trajectories and benefit from an additional boost. As shown in Fig. 1(d), swimmers with lower aspect ratio then naturally reach the target faster and this effect is amplified when decreasing the swimmer speed.

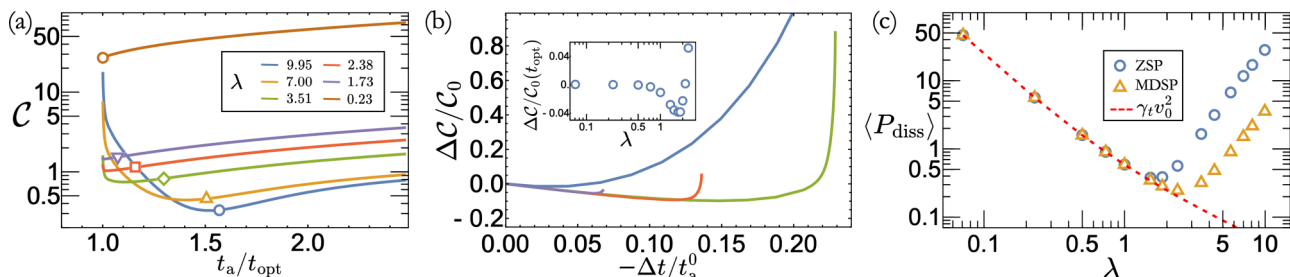


FIG. 2. Energy efficiency of navigating swimmers. (a) Cost associated with optimal trajectories as function of the travel time for several values of the aspect ratio. t_a is normalized by the optimal value achieved by ZSP. Symbols indicate the values t_a^0 and C_0 obtained in absence of active steering. (b) Relative cost variation as function of the relative travel time improvement with respect to the nonsteering case [see text for definitions; same legend as in (a)]. Inset: ΔC as function of the swimmer aspect ratio for $t_a = t_{\text{opt}}$. (c) Comparison between the trajectory-averaged dissipated power resulting from the optimal control (orange triangles) and the compensating protocol ω_a^c (blue circles) as function of the aspect ratio for $t_a = t_{\text{opt}}$.

In fact, Eq. (1) with $\omega_a = \mathbf{0}$ and $\lambda \rightarrow 0$ ($\alpha = -1$) corresponds to the minimum travel time policy for point-like swimmers, i.e., ZSP [35]. Therefore, thanks to passive rotations from the flow a thin disk-shaped particle self-propelling along its axis of symmetry always follows time-optimal trajectories without the need to actively steer. Although t_a^0 generally increases with the aspect ratio, the required power to put the swimmer into motion—here set by the coefficient $\gamma_t(\lambda)$ —is a decreasing function of λ [Fig. 1(c)]. These opposing trends hence imply the existence of a finite optimal aspect ratio λ_{opt} that minimizes the overall cost C_0 . Consistently, for the linear shear flow considered here, λ_{opt} is a decreasing function of σ (increasing function of v_0), as reported in Fig. 1(e).

IV. NAVIGATION OF “SMART” SWIMMERS: THE COST OF STEERING

So far, we have focused on swimmers that are passively rotated by the flow and have shown that their geometry alone introduces a trade-off between energy and travel time optimization. We now discuss how this trade-off impacts the navigation performances of actively steering swimmers. The optimal protocol for the control ω_a that minimizes the cost (2) is determined using OCT [41,45]. Defining \mathbf{p} and $\mathbf{p}_{\hat{u}}$ as the Lagrange multipliers enforcing Eq. (1), it follows from Pontryagin’s minimization principle that the optimal value of the control is obtained from $\nabla_{\omega_a} \mathcal{H} = \mathbf{0}$ with the effective Hamiltonian $\mathcal{H} \equiv P_{\text{diss}} + \sigma + \mathbf{p} \cdot \dot{\mathbf{r}} + \mathbf{p}_{\hat{u}} \cdot \dot{\hat{u}}$, leading to $\omega_a = (\mathbf{p}_{\hat{u}} \times \hat{u})/[2s^2\gamma_t(\lambda)]$. The dynamics of the momenta are in turn given by

$$\dot{\mathbf{p}} = -\nabla_r \mathcal{H} = -\nabla_r [\mathbf{p} \cdot \mathbf{f}(\mathbf{r}) + \mathbf{p}_{\hat{u}} \cdot (\omega_f \times \hat{u})], \quad (3a)$$

$$\dot{\mathbf{p}}_{\hat{u}} = -\nabla_{\hat{u}} \mathcal{H} = -v_0 \mathbf{p} - \nabla_{\hat{u}} [\mathbf{p}_{\hat{u}} \cdot (\omega_f \times \hat{u})]. \quad (3b)$$

The minimum dissipation steering protocol (MDSP) is then obtained by integrating the dynamics of $(\mathbf{r}, \hat{u}, \mathbf{p}, \mathbf{p}_{\hat{u}})$ with boundary conditions that depend on the navigation problem of interest (details about OCT and numerical methods are given in Appendix A). For the point-to-point navigation in a shear flow with unspecified initial and final particle orientations introduced in the previous section, the initial and final values of \mathbf{p} need to be determined, while $\mathbf{r}(0) = \mathbf{r}_0$, $\mathbf{r}(t_a) = \mathbf{r}_T$, and $\mathbf{p}_{\hat{u}}(0) = \mathbf{p}_{\hat{u}}(t_a) = \mathbf{0}$.

In the presence of active steering, the optimization problem additionally depends on the (dimensionless) swimmer size s . Since actively steering swimmers can in principle reach the target in a time $t_a \neq t_a^0(\lambda)$, we now set $\sigma = 0$ and directly use t_a as a control parameter. Additionally, we set $s = 0.1$ and $v_0 = 1/8$, thus focusing on the most relevant regime where the swimmer size and self-propulsion strength are lower than the characteristic velocity and length scale of the flow. We checked that these choices do not qualitatively influence our results. Below, we characterize the navigation performance of the swimmer varying the remaining two parameters t_a and λ .

Figure 2(a) displays the dimensionless cost \mathcal{C} associated with optimal trajectories as a function of the arrival time t_a for several values of λ . As they actively steer, navigating swimmers can now reach the target in a time lower than t_a^0 [indicated by the symbols in Fig. 2(a)]. Remarkably, for all shapes the accessible arrival times extend to the minimum value t_{opt} achieved for $\lambda \rightarrow 0$ in the absence of control. Although for $t_a > t_a^0$ the cost decreases monotonically with λ , the regime $t_a < t_a^0$ exhibits nontrivial crossovers with needle-shaped swimmers becoming increasingly less energy efficient at smaller times. Hence, the optimal shape of navigating swimmers generally depends on the prescribed trajectory time.

Focusing on the regime $t_a \leq t_a^0$, we show in Fig. 2(b) the relative cost variation $\Delta C \equiv (\mathcal{C} - C_0)$ associated with a relative travel time improvement $\Delta t \equiv (t_a - t_a^0)$. The initial decrease of ΔC with $-\Delta t$ attests that, although the swimmer has to actively steer in order to reach the target in a time $t_a \lesssim t_a^0$, it does so while spending *less* energy. This feature, which we expect to hold generally, can be understood from the expression of the cost: $\mathcal{C} = \int_0^{t_a} d\tau [\gamma_t(\lambda)v_0^2 + s^2\gamma_r(\lambda)|\omega_a|^2]$. While it is reasonable to assume that for $t_a \approx t_a^0$ the control amplitude $|\omega_a| \simeq |t_a - t_a^0|$, such that the contribution to \mathcal{C} of the active steering $\simeq (t_a - t_a^0)^2$, the translational dissipation decreases linearly with t_a . Therefore, so long as the swimmer travels over distances much larger than its size ($s \ll 1$), the cost increase resulting from active steering remains subdominant for $t_a \lesssim t_a^0$. As $t_a^0 \rightarrow t_{\text{opt}}$ for decreasing λ , spherical or disk-shaped swimmers can then keep saving energy when optimizing their travel time down to t_{opt} . For the navigation setup considered here, we find that such scenario occurs for $\lambda \lesssim 2$ [inset of Fig. 2(b)], while $\Delta C/C_0$ at $t_a = t_{\text{opt}}$ exhibits a minimum at $\lambda \simeq 1.73$.

As MDSP is able to provide the minimum time trajectories naturally followed by disk-like swimmers, it is instructive to compare it with a naive implementation of ZSP. Namely, we consider a control $\omega_a^c(\lambda) \equiv \omega_f(\lambda = 0) - \omega_f(\lambda)$ that compensates for the shape-dependent hydrodynamic rotations and implements the steering protocol minimizing travel time for a point-like swimmer. As shown in Fig. 2(c), for needle-like swimmers following MDSP the average dissipated power $\langle P_{\text{diss}} \rangle \equiv C/t_a$ is about an order of magnitude lower than that associated with the simpler compensating control ω_a^c . Conversely, for disk-like swimmers which barely steer, $\langle P_{\text{diss}} \rangle \approx \gamma_t v_0^2$ in both cases.

V. NAVIGATION IN A COMPLEX ENVIRONMENT

We now discuss how the above results extend beyond the restricted setting of point-to-point navigation by generalizing our approach to the case of a stationary two-dimensional Gaussian random flow with characteristic intensity v_f and correlation length ℓ . Namely, the random flow is defined from a random stream function $\psi(\mathbf{r})$ having zero mean and Gaussian correlations [46]: $\langle \psi(\mathbf{r})\psi(\mathbf{r}') \rangle = \frac{1}{2}\ell^2 v_f^2 e^{-|\mathbf{r}-\mathbf{r}'|^2/(2\ell^2)}$. For the simulation results shown below, a single instance of the random flow in a periodic square domain of length $L = 25$ was generated (details in Appendix C).

Taking inspiration from tactic behaviors of some biological and synthetic microswimmers, which are able to preferably move against gravity or along gradients of, e.g., chemicals or light intensity [21–24,47], we study here a more realistic navigation problem requiring the swimmer to travel from an initial position on a vertical line at $x = 0$ to a finish line located at $x = 4L$ [see Fig. 3(a)]. In order to account for this new navigation task, we revised the cost function as $C_{\text{RF}} \equiv -\kappa[x(t_a) - x(0)] + \int_0^{t_a} d\tau P_{\text{diss}}$, where the $\propto \kappa$ boundary term is intended to maximize the displacement along the direction set by the tactic response. Using dimensionless units, we are left with 4 parameters: λ , v_0 , s , and κ . From OCT, the revised MDSP for a given initial position \mathbf{r}_0 is then obtained by integrating Eqs. (1) and (3) with boundary conditions $\mathbf{r}(0) = \mathbf{r}_0$, $\mathbf{p}(t_a) = -\kappa\hat{\mathbf{x}}$, and $\mathbf{p}_{\hat{\mathbf{u}}}(0) = \mathbf{p}_{\hat{\mathbf{u}}}(t_a) = \mathbf{0}$. However, in practice solving such boundary value problem using, e.g., shooting methods, in a complex flow turns out to be computationally unfeasible due to the chaotic nature of the solutions [30,48].

Here, we have instead designed an alternative approach that locally approximates MDSP and whose derivation is detailed in Appendix B. Namely, we define a time horizon τ [31] which we assume sufficiently small such that \mathbf{r} and $\hat{\mathbf{u}}$ do not significantly vary over the interval $[0; \tau]$. Within this assumption, Eqs. (3) reduce to a linear system of differential equations which we can solve exactly. Given a swimmer with specified position and orientation at time t , we thus solve the optimization problem over the interval $[t; t + \tau]$ by determining the values of $\mathbf{p}(t)$ and $\mathbf{p}_{\hat{\mathbf{u}}}(t)$ from the solution of (3) and the conditions $\mathbf{p}(t + \tau) = -\kappa\hat{\mathbf{x}}$ and $\mathbf{p}_{\hat{\mathbf{u}}}(t + \tau) = \mathbf{0}$. This way, we obtain an approximation of the optimal control $\omega_a(t)$ that minimizes the navigation cost at fixed τ . The limit $\tau \rightarrow 0$ amounts to ignoring the presence of the flow field, such that it leads to simple taxis toward the target line. Conversely, for large τ the approximation of a locally uniform environment becomes increasingly poor. In practice, the intermediate optimal value

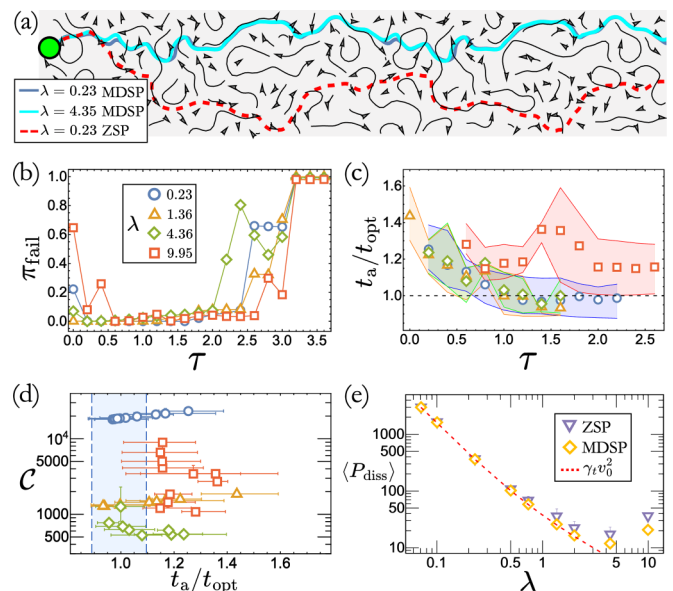


FIG. 3. Optimal navigation in a Gaussian random flow. (a) Three exemplary trajectories with travel time $t_a \approx t_{\text{opt}}$ starting from the same point (green dot) and obtained from the local approximations of ZSP (dashed red curve) and MDSP (solid curves). The displayed domain size is $2L \times L/2$ and the black arrows show the local direction of the flow. (b) Probability of not reaching the finish line as function of τ for four different aspect ratios λ . (c) Mean travel time t_a as function of τ . The shaded intervals show the first and third quartiles while the dotted line indicates the reference value t_{opt} . (d) Mean cost of navigation as function of the arrival time. Error bars correspond to the first and third quartiles, while the shaded area indicates the interval of confidence on t_{opt} . Legends for (c) and (d) are the same as in (b). (e) Comparison between the average dissipated power of the approximated MDSP and ZSP at arrival time $t_a \approx t_{\text{opt}}$ as function of the swimmer aspect ratio.

of τ is determined empirically. Similar optimization protocols have been implemented in Refs. [31,49]. The particularity of the approach we propose is that it is generalizable to any optimal control problem sharing a similar Hamiltonian structure as discussed in Appendix A. In fact, applying it to the Zermelo problem we recover the protocol derived in [31]. Importantly, the resulting navigation strategy can be implemented solely from local measurements of the environment such as the preferred direction of taxis and flow gradients, which correspond to information available to certain microswimmers [21,50,51]. Consequently, contrary to trajectory planning [29], this policy is also robust to the presence of fluctuations, as further demonstrated in the next section.

As they do not strongly influence the results, we set $v_0 = 1$, $s = 0.1$, and $\kappa\tau v_0 = 10^2$. Figure 3(a) shows representative trajectories obtained from the local approximations of MDSP and ZSP. In both cases, they end up on an attractor after crossing typically one or two system sizes L along the x direction. The number of reachable attractors depends on the policy employed. To account for all of them, all data were collected by averaging over the initial swimmer position $\mathbf{r}_0 = (0, y_0)$ with y_0 uniformly distributed in $[0; L]$.

Since for some parameters swimmers might get trapped in strong flow regions, we define π_{fail} as the probability that

a swimmer does not reach the finish line in a finite simulation time. As shown in Fig. 3(b), for MDSP π_{fail} exhibits a minimum in the range $0.5 \lesssim \tau \lesssim 2$ for all values of λ . Measuring the average arrival time of trajectories that successfully reach the target line, we find that it is generally minimal within a similar range of τ values [Fig. 3(c)]. A similar trend is observed for ZSP, and we use the corresponding minimum arrival time $t_{\text{opt}} \approx 0.7 \times (4L/v_0)$ as a reference value. In agreement with results obtained in the simple shear flow, for most aspect ratios there exists a value $\tau \approx 1$ for which t_a obtained from MDSP is comparable to t_{opt} [Fig. 3(c)]. Comparing Figs. 3(d) and 3(e) with Figs. 2(a) and 2(c) further confirms the similarities between the two sets of results. Namely, we observe the selection of finite optimal aspect ratio set by the arrival time. Moreover, for $t_a \approx t_{\text{opt}}$ MDSP systematically performs better than ZSP while the two converge as $\lambda \rightarrow 0$ where they satisfy $\langle P_{\text{diss}} \rangle \approx \gamma_r(\lambda)v_0^2$.

VI. THE EFFECT OF ROTATIONAL DIFFUSION

As the motion of swimmers at microscopic scales is affected by the presence of fluctuations coming from diffusion or tumbles in the direction of motion, we also checked the robustness and generality of the results presented in the previous section by including this ingredient in the simulations. Namely, we integrate the locally approximated MDSP and ZSP with the same parameters as those used to analyze the navigation in random flow, while also including orientational diffusion of the swimmer's orientation with a (dimensionless) rotational diffusivity $D_r = 1$ (details about the numerical methods are given in Appendix C).

Our simulation results are summarized in Fig. 4. To ease the comparison with the deterministic case, the quantities reported in the four panels therein correspond to the ones in Figs. 3(b)–3(e). First, it is clear that the presence of noise in the swimmer orientational dynamics does not qualitatively affect the conclusions presented above. Figure 4(a) indeed demonstrates the existence of a range $0.5 \lesssim \tau \lesssim 2$ for which the probability π_{fail} that the swimmer does not reach the target line remains small regardless of the swimmer shape. In fact, for some values of τ the probability π_{fail} may even be *smaller* than in the absence of noise. This suggests that rotational diffusion may help the swimmers to exit traps induced by the flow structure [30], thus resulting in a higher success rate.

Meanwhile, swimmers of any shape following MDSP are still able to reach, on average, the finish line in a time comparable to the one achieved with ZSP in the same setup [Fig. 4(b); note that t_{opt} here is around 10% larger than the minimum arrival time in the absence of noise]. While the variations of the navigation cost with arrival time and aspect ratio are similar with and without rotational diffusion, its presence leads to a systematic increase of dissipation [compare Figs. 4(c) and 3(d)]. Here too, the optimal aspect ratio minimizing energetic dissipation is therefore finite. Furthermore, a comparison of Figs. 4(d) and 3(e) reveals that the presence of rotational diffusion has a much more dramatic impact on the performances of ZSP than that of MDSP for all simulated aspect ratios. These results thus suggest that taking into account the coupling of the swimmer's body geometry

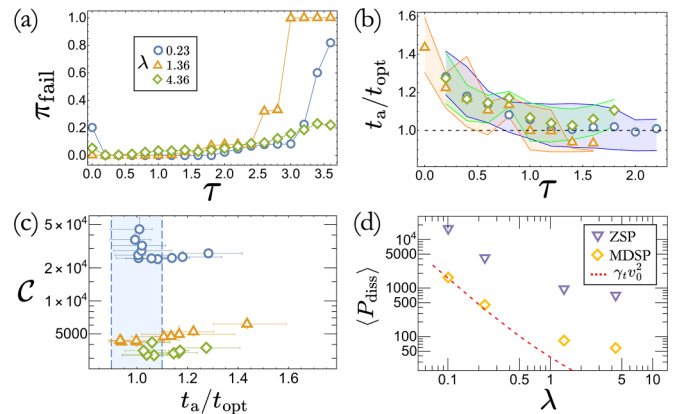


FIG. 4. Performance of swimmers navigating in a Gaussian random flow while following ZSP and MDSP in the presence of rotational diffusion (parameters are the same as in Fig. 3). (a) Probability of not reaching the target line as function of τ for three different aspect ratios λ . (b) Mean travel time t_a vs τ . The shaded intervals show the first and third quartiles, while the dotted line indicates the mean time taken by a swimmer following ZSP. (c) Mean cost of navigation as function of the arrival time. Error bars show the first and third quartiles, while the shaded area indicates the interval of confidence on t_{opt} . Legends for (b) and (c) are the same as (a). (d) Comparison between the average dissipated power of the approximated MDSP and ZSP at arrival time $t_a \approx t_{\text{opt}}$ as function of the swimmer aspect ratio λ .

with hydrodynamics may help for the design of policies more robust to fluctuations.

VII. DISCUSSION

We have studied how the body geometry of microswimmers influences their navigation performances. Our analysis reveals that while disk-shaped swimmers navigate efficiently without needing to actively steer, they also dissipate more energy for propulsion. This general feature leads to the selection of a finite optimal aspect ratio minimizing the overall cost of navigation, and offers microswimmers having limited control over their swimming direction an alternative strategy to optimize travel time and energy dissipation.

We have moreover shown that the MDSP policy ensuring minimum dissipation provides time-optimal trajectories associated with a systematically lower energy cost than achieved with a naive generalization of ZSP, while it is also more robust to fluctuations. Overall, as these conclusions were found to be insensitive to the details of the navigation setting, we expect them to be relevant to practical situations including planktonic navigation in turbulent flows [50–52] or the maximization of encounter rates of microswimmers with food sources [40,53], while they may also find application to the design of smart artificial swimmers [12].

ACKNOWLEDGMENTS

We thank Tarun Mascarenhas for discussions at the early stages of this work. L.P. is thankful for the funding from the International Max Planck Research School (IMPRS) for the Physics of Biological and Complex Systems, and for the

partial support from the European Research Council (ERC) under the European Union's Horizon 2020 research and innovation program (Grant Agreement No. 882340). A.V. acknowledges support from the Slovenian Research Agency (Grant No. P1-0099). This work has received support from the Max Planck School Matter to Life and the MaxSynBio Consortium, which are jointly funded by the Federal Ministry of Education and Research (BMBF) of Germany, and the Max Planck Society.

APPENDIX A: DETAILS ON OCT AND NUMERICAL SOLUTIONS OF THE OPTIMIZATION PROBLEMS

Let us consider a generic navigation problem where the swimmer state is parametrized by the vector $\mathbf{q}(t) = (q_1(t), \dots, q_n(t))$ whose deterministic evolution follows $\dot{\mathbf{q}} = \mathbf{L}[\mathbf{q}(t), \mathbf{c}(t), t]$, where \mathbf{c} denotes the control that can be used for navigation. In this work, for instance, $\mathbf{q} = (\mathbf{r}, \hat{\mathbf{u}})$ and \mathbf{L} is defined by Eq. (1). The navigation task consists in finding the trajectory minimizing the cost function,

$$\mathcal{C} = \phi(\mathbf{q}(t_a), t_a) + \int_0^{t_a} \mathcal{L}[\mathbf{q}(t), \mathbf{c}(t), t] dt, \quad (\text{A1})$$

with boundary conditions $q_i(0) = q_{i,0}$ and $q_j(t_a) = q_{j,T}$, where the indices $1 \leq i \leq k$ and $m \leq j \leq l$ such that for $k, l < n$ or $m > 1$ certain degrees of freedom can be unspecified at the two ends of the trajectory. ϕ and \mathcal{L} in (A1) are respectively known as the end point and running costs. OCT recasts this optimization problem into a boundary value problem for the dynamical system [54],

$$\dot{\mathbf{q}} = \nabla_{\mathbf{p}} \mathcal{H}, \quad \dot{\mathbf{p}} = -\nabla_{\mathbf{q}} \mathcal{H}, \quad (\text{A2})$$

where the Hamiltonian $\mathcal{H} \equiv \mathcal{L}[\mathbf{q}(t), \mathbf{c}(t), t] + \mathbf{p}(t) \cdot \mathbf{L}[\mathbf{q}(t), \mathbf{c}(t), t]$ and with the boundary conditions

$$\begin{aligned} q_i(0) &= q_{i,0}, & 1 \leq i \leq k \text{ (specified)}, \\ p_i(0) &= 0, & k < i \leq n \text{ (unspecified)}, \\ q_j(t_a) &= q_{j,T}, & m \leq j \leq l \text{ (specified)}, \\ p_j(t_a) &= \partial_{q_j} \phi, & 1 \leq j < m \wedge l < j \leq n \text{ (unspecified)}. \end{aligned}$$

In addition, the navigation policy for the control is obtained by minimizing the Hamiltonian, $\nabla_{\mathbf{c}} \mathcal{H} = 0$, while an unspecified arrival time t_a leads to the additional condition on the Hamiltonian, $\mathcal{H}(t_a) = -\partial_t \phi|_{t_a}$. For the navigation problems considered in the main text, this second condition always reduces to $\mathcal{H} = 0$, where \mathcal{H} is a constant of motion. For convenience, throughout this work we numerically solve the optimization at fixed t_a by relaxing the constraint on \mathcal{H} . Varying t_a as a parameter, its value for which the total cost (2) is minimized then also corresponds to $\mathcal{H} = 0$ [54].

The correspondence between the general optimization problem and the two navigation protocols addressed in the text is summarized in Table I. For the study of navigation in linear shear flow, we solved the boundary value problem via standard shooting methods. Namely, given a trajectory time t_a and a guess for the n unknown initial conditions $(\{q_i(0)\}_{i \in [k+1;n]}; \{p_i(0)\}_{i \in [1;k]})$, the coupled systems of ordinary differential equations of (A2) are integrated via the 4th-order Runge-Kutta method with time step $dt = 10^{-5}$.

TABLE I. Correspondence between the general formulation of optimal navigation and the two policies studied in the main text.

Problem	ZSP (minimum time)	MDSP (minimum dissipation)
State variables (\mathbf{q})	\mathbf{r}	$\mathbf{r}, \hat{\mathbf{u}}$
Conjugate variables	$\mathbf{p} \leftrightarrow \mathbf{r}$	$\mathbf{p} \leftrightarrow \mathbf{r}, \mathbf{p}_{\hat{\mathbf{u}}} \leftrightarrow \hat{\mathbf{u}}$
Optimal control (\mathbf{c})	$\hat{\mathbf{u}} = -\mathbf{p}/ \mathbf{p} $	$\omega_{\hat{\mathbf{u}}} \propto (\mathbf{p}_{\hat{\mathbf{u}}} \times \hat{\mathbf{u}})$
Running cost (\mathcal{L})	σ	$P_{\text{diss}} + \sigma$

The initial conditions are then iterated using the routine `GSL_MULTIROOT_FSOLVER_HYBRIDS` provided by the GSL library [55] to determine the roots of the system $(\{q_j(t_a) - q_{j,T}\}_{j \in [m;l]}; \{p_j(t_a) - \partial_{q_j} \phi\}_{j \in [1;m-1] \cup [l+1;n]})$. This process is then iterated until reaching convergence, which we define as when the sum of absolute errors falls under a specified threshold (here set to 10^{-6}).

APPENDIX B: THE APPROXIMATE NAVIGATION POLICIES

Here, we give additional details about the derivation of the approximate navigation policies described in the text. To keep the presentation simple, we restrict the problem to two dimensions for which the equations of motion simplify as

$$\dot{\mathbf{r}} = v_0 \hat{\mathbf{u}}(\theta) + \mathbf{f}(\mathbf{r}), \quad (\text{B1a})$$

$$\dot{\theta} = \omega_a + \omega_f(\mathbf{r}, \theta), \quad (\text{B1b})$$

$$\dot{\mathbf{p}} = -\nabla_{\mathbf{r}}[\mathbf{p} \cdot \mathbf{f}(\mathbf{r}) + p_{\theta} \omega_f(\mathbf{r}, \theta)], \quad (\text{B1c})$$

$$\dot{p}_{\theta} = -v_0 \mathbf{p} \cdot \hat{\mathbf{u}}^{\perp}(\theta) - \partial_{\theta}[p_{\theta} \omega_f(\mathbf{r}, \theta)], \quad (\text{B1d})$$

where $\hat{\mathbf{u}}^{\perp}(\theta) \equiv d\hat{\mathbf{u}}(\theta)/d\theta$ and, in dimensionless units, $\omega_a = -p_{\theta}/(2s^2\gamma_r)$.

Given a swimmer with position \mathbf{r} and orientation θ at time t , we wish to determine the control $\omega_a(t)$ that minimizes the cost $\mathcal{C}_{\text{RF}} = -\kappa[x(t_a) - x(t)] + \int_t^{t_a} d\tau P_{\text{diss}}$. From OCT, the optimal control is obtained solving the boundary value problem for the system (B1) with the end-point conditions $\mathbf{p}(t_a) = -\kappa \hat{\mathbf{x}}$ and $p_{\theta}(t_a) = 0$. Since the solutions of (B1) are generally chaotic in the presence of strong or complex flows [30], shooting methods do not necessarily converge. Hence, reinforcement learning-based approaches have become increasingly popular to address similar scenarios [26,32,48,52,56–58]. Here, instead, we opt for a more systematic approach by deriving an approximation for $\omega_a(t)$ that relies only on the information locally available to the swimmer.

Denoting $\mathbf{P} \equiv (\mathbf{p}, p_{\theta})$, the dynamics of the conjugate variables can be written as $\dot{\mathbf{P}} = -\mathbf{M} \cdot \mathbf{P}$ where the time-dependent coefficient matrix reads

$$\mathbf{M} \equiv \begin{pmatrix} F_{11} & F_{12} & \Upsilon_1 \\ F_{21} & F_{22} & \Upsilon_2 \\ -v_0 \sin \theta & v_0 \cos \theta & \Upsilon_3 \end{pmatrix},$$

with

$$\mathbf{F} \equiv \begin{pmatrix} \partial_x f_x & \partial_x f_y \\ \partial_y f_x & \partial_y f_y \end{pmatrix}, \quad \Upsilon \equiv \begin{pmatrix} \partial_x \omega_f \\ \partial_y \omega_f \\ \partial_{\theta} \omega_f \end{pmatrix}.$$

We now assume that the variations of \mathbf{r} and θ are sufficiently smooth such that there exists a timescale τ over which the coefficients of the matrix \mathbf{M} are nearly constant. Under this assumption, the solution for \mathbf{P} is readily obtained for $t' \in [t; t + \tau]$ as

$$\mathbf{P}(t') \simeq e^{-(t'-t)\mathbf{M}} \cdot \mathbf{P}(t), \quad (\text{B2})$$

where the coefficients of the matrix \mathbf{M} are evaluated at time t . Optimizing the cost \mathcal{C}_{RF} over this time window then imposes that $P_i(t + \tau) = -\kappa \delta_{i,1}$ which, together with Eq. (B2), leads to the initial value $P_j(t) \simeq -\kappa \delta_{k,1} e^{\tau M_{jk}}$ (summation over repeated indices is implied). Now using the relationship between ω_a and p_θ we finally get

$$\omega_a(t) = -\frac{p_\theta(t)}{2s^2\gamma_r} \simeq \frac{\kappa}{2s^2\gamma_r} e^{\tau M_{31}}. \quad (\text{B3})$$

Integrating Eqs. (B1a) and (B1b) with Eq. (B3), we thus obtain an approximation of MDSP based on the local information about the environment stored in the coefficients of the matrix \mathbf{M} .

Expanding the matrix exponential up to leading order terms in τ , the policy (B3) reduces to

$$\omega_a = -\frac{\kappa v_0 \tau}{2s^2\gamma_r} \sin \theta + O(\tau^2). \quad (\text{B4})$$

For small values of τ , the policy amounts to assuming a uniform environment such that the swimmer points straight toward the finish line. On the other hand, the higher-order contributions to (B4) depend on the flow structure and thus allow for smart navigation.

A local approximation of ZSP can be obtained similarly to the above derivation for MDSP. As described in Table I, since in this case the swimmer is assumed point-like the state variable is the particle position \mathbf{r} while the control is the steering direction $\hat{\mathbf{u}}$. Applying OCT to this problem with the cost $\mathcal{C}_{\text{ZSP}} = -\kappa[x(t_a) - x(t)] + \sigma(t_a - t)$, we obtain

$$\dot{\mathbf{p}} = -\mathbf{F} \cdot \mathbf{p}, \quad \hat{\mathbf{u}} = -\frac{\mathbf{p}}{|\mathbf{p}|}, \quad (\text{B5})$$

with the boundary condition $\mathbf{p}(t_a) = -\kappa \hat{\mathbf{x}}$. Following the same procedure that led from Eqs. (B1) to Eq. (B3), we assume the matrix \mathbf{F} to be constant over the time interval $[t; t + \tau]$, such that after solving for \mathbf{P} we get

$$\hat{\mathbf{u}}(t) = \frac{e^{\tau \mathbf{F}} \cdot \hat{\mathbf{x}}}{|e^{\tau \mathbf{F}} \cdot \hat{\mathbf{x}}|}, \quad (\text{B6})$$

where \mathbf{F} is evaluated at time t . As previously, the leading order contribution to Eq. (B6) leads to $\mathbf{u}(t) = \hat{\mathbf{x}} + O(\tau)$, i.e., pointing straight at the finish line, while contributions from the flow show up at higher order. We note that (B6) was derived via a different method in Ref. [31].

Equation (B6) describes instantaneous reorientations of the swimmer directions. Hence, to compare the performances of ZSP and MDSP in Fig. 3 we implemented an underdamped version of (B6) obtained by simulating Eqs. (B1a) and (B1b)

with the control

$$\omega_{a,\text{ZSP}} = -\frac{v_0 \kappa \tau}{2s^2 \gamma_r} \sin(\theta - \theta_{\text{ZSP}}), \quad (\text{B7})$$

where θ_{ZSP} denotes the orientation set by (B6).

APPENDIX C: NUMERICAL METHODS

1. Navigation in a Gaussian random flow

The Gaussian random flow described in the main text and sketched in Fig. 3(a) was obtained via the power spectrum generation method [59]. We first built an $N \times N$ matrix of uncorrelated zero mean and unit variance Gaussian white noise, and then evaluated its Fourier transform. We multiplied the outcome by the square root of the desired power spectrum of the stream function $\psi(\mathbf{r})$ —the Fourier transform of its correlation function—and Fourier transform the result back. Finally, the flow field is obtained using finite difference via $\mathbf{f}(\mathbf{r}) = 2^{-1/2} \nabla \times [\hat{\mathbf{z}} \psi(\mathbf{r})]$ where $\hat{\mathbf{z}}$ is the out-of-plane unit vector. The flow generated this way is by construction periodic across the domain boundaries. We used $N = 2500$ and a physical system size $L = 25$ (in units of ℓ), leading to a spatial resolution of $dx = 10^{-2}$. For simulations in the random flow, the equations of motion of the swimmer (1) were numerically integrated together with the equation for the control [i.e., Eq. (B3) for MDSP and Eq. (B7) for ZSP] with a 4th-order Runge-Kutta method and a time step $dt = 10^{-4}$. The matrix exponentials in (B3) and (B7) were computed with the GSL_LINALG_EXPONENTIAL_SS routine from the GSL library [55].

The results presented in the main text have been obtained from simulations of $N_{\text{ic}} = 10^3$ trajectories with initial positions $\mathbf{r}_0 = y_0 \hat{\mathbf{y}}$ and y_0 uniformly distributed in $\in [0, L]$. For convenience and because its specific value does not affect the convergence of the trajectories to the attractors mentioned in the main text [see also Fig. 3(a)], the initial heading direction of the swimmer is set to $\theta_0 = 0$. The probability π_{fail} that a swimmer does not reach the finish line located at $x = 4L$ is defined as the fraction of trajectories not crossing it within a time $t_{\text{max}} = 5 \times 4L/v_0$. The mean and quartiles of both arrival time (t_a) and dissipated energy (\mathcal{C}) were computed considering only the trajectories that successfully reach the finish line, while the data points shown in Figs. 3(c) and 3(d) in the main text all satisfy $\pi_{\text{fail}} \leq 0.05$.

2. Langevin simulations

As a minimal extension of the deterministic equation of motion (1), we considered the following two-dimensional Langevin equations including rotational diffusion with corresponding strength D_r (here expressed in units of v_f/ℓ), which we moreover set to 1:

$$\begin{aligned} \dot{\mathbf{r}} &= v_0 \hat{\mathbf{u}}(\theta) + \mathbf{f}(\mathbf{r}), \\ \dot{\theta} &= \omega_a + \omega_f(\mathbf{r}, \theta) + \sqrt{2D_r} \xi_\theta, \end{aligned} \quad (\text{C1})$$

where ξ_θ is a delta-correlated Gaussian white noise with unit variance, while the angular velocity ω_f induced by hydrodynamic torques is defined in the main text. The active control ω_a depends on the policy considered. Here, we used the expressions derived in Appendix B, namely Eq. (B3) for the

minimum dissipation steering policy (MDSP) and Eq. (B7) for the Zermelo steering policy (ZSP, corresponding to minimal time). These equations together with Eq. (C1) were integrated

by means of an Euler-Mayurama scheme with a time step $dt = 10^{-4}$, while convergence with respect to time discretization was checked.

-
- [1] L. T. Nielsen and T. Kjørboe, Foraging trade-offs, flagellar arrangements, and flow architecture of planktonic protists, *Proc. Natl. Acad. Sci. USA* **118**, 71 (2021).
- [2] D. Bray, *Cell Movements* (Garland Science, 2000).
- [3] J. Elgeti, R. G. Winkler, and G. Gompper, Physics of microswimmers—single particle motion and collective behavior: a review, *Rep. Prog. Phys.* **78**, 056601 (2015).
- [4] J. G. Mitchell, The energetics and scaling of search strategies in bacteria, *Am. Nat.* **160**, 727 (2002).
- [5] S. Tavaddod, M. A. Charsooghi, F. Abdi, H. R. Kholesifard, and R. Golestanian, Probing passive diffusion of flagellated and deflagellated *Escherichia coli*, *Eur. Phys. J. E* **34**, 16 (2011).
- [6] H. C. Berg, *E. Coli in Motion* (Springer Science and Business Media, New York, NY, 2008).
- [7] E. M. Purcell, Life at low Reynolds number, *Am. J. Phys.* **45**, 3 (1977).
- [8] S. Chattopadhyay, R. Moldovan, C. Yeung, and X. L. Wu, Swimming efficiency of bacterium *Escherichia coli*, *Proc. Natl. Acad. Sci. USA* **103**, 13712 (2006).
- [9] J. S. Guasto, R. Rusconi, and R. Stocker, Fluid mechanics of planktonic microorganisms, *Annu. Rev. Fluid Mech.* **44**, 373 (2012).
- [10] Y. Katsu-Kimura, F. Nakaya, S. A. Baba, and Y. Mogami, Substantial energy expenditure for locomotion in ciliates verified by means of simultaneous measurement of oxygen consumption rate and swimming speed, *J. Exp. Biol.* **212**, 1819 (2009).
- [11] J. R. Taylor and R. Stocker, Trade-offs of chemotactic foraging in turbulent water, *Science* **338**, 675 (2012).
- [12] A. C. H. Tsang, E. Demir, Y. Ding, and O. S. Pak, Roads to smart artificial microswimmers, *Adv. Intell. Syst.* **2**, 1900137 (2020).
- [13] N. Osterman and A. Vilfan, Finding the ciliary beating pattern with optimal efficiency, *Proc. Natl. Acad. Sci. USA* **108**, 15727 (2011).
- [14] A. Vilfan, Optimal shapes of surface slip driven self-propelled microswimmers, *Phys. Rev. Lett.* **109**, 128105 (2012).
- [15] J. Elgeti and G. Gompper, Emergence of metachronal waves in cilia arrays, *Proc. Natl. Acad. Sci. USA* **110**, 4470 (2013).
- [16] H. Guo, H. Zhu, R. Liu, M. Bonnet, and S. Veerapaneni, Optimal slip velocities of micro-swimmers with arbitrary axisymmetric shapes, *J. Fluid Mech.* **910**, A26 (2021).
- [17] A. Daddi-Moussa-Ider, B. Nasouri, A. Vilfan, and R. Golestanian, Optimal swimmers can be pullers, pushers or neutral depending on the shape, *J. Fluid Mech.* **922**, R5 (2021).
- [18] P. Giri and R. K. Shukla, Optimal transport of surface-actuated microswimmers, *Phys. Fluids* **34**, 043604 (2022).
- [19] B. Nasouri, A. Vilfan, and R. Golestanian, Minimum dissipation theorem for microswimmers, *Phys. Rev. Lett.* **126**, 034503 (2021).
- [20] A. Daddi-Moussa-Ider, R. Golestanian, and A. Vilfan, Minimum entropy production by microswimmers with internal dissipation, *Nat. Commun.* **14**, 6060 (2023).
- [21] J. D. Wheeler, E. Secchi, R. Rusconi, and R. Stocker, Not just going with the flow: The effects of fluid flow on bacteria and plankton, *Annu. Rev. Cell Dev. Biol.* **35**, 213 (2019).
- [22] G. Jékely, Evolution of phototaxis, *Philos. Trans. R. Soc. London B* **364**, 2795 (2009).
- [23] H. C. Berg and D. A. Brown, Chemotaxis in *Escherichia coli* analysed by three-dimensional tracking, *Nature (London)* **239**, 500 (1972).
- [24] R. R. Bennett and R. Golestanian, A steering mechanism for phototaxis in *Chlamydomonas*, *J. R. Soc. Interface* **12**, 20141164 (2015).
- [25] B. Liebchen and H. Löwen, Optimal navigation strategies for active particles, *Europhys. Lett.* **127**, 34003 (2019).
- [26] E. Schneider and H. Stark, Optimal steering of a smart active particle, *Europhys. Lett.* **127**, 64003 (2019).
- [27] A. Daddi-Moussa-Ider, H. Löwen, and B. Liebchen, Hydrodynamics can determine the optimal route for microswimmer navigation, *Commun. Phys.* **4**, 15 (2021).
- [28] L. Piro, E. Tang, and R. Golestanian, Optimal navigation strategies for microswimmers on curved manifolds, *Phys. Rev. Res.* **3**, 023125 (2021).
- [29] L. Piro, B. Mahault, and R. Golestanian, Optimal navigation of microswimmers in complex and noisy environments, *New J. Phys.* **24**, 093037 (2022).
- [30] L. Piro, R. Golestanian, and B. Mahault, Efficiency of navigation strategies for active particles in rugged landscapes, *Front. Phys.* **10**, 1034267 (2022).
- [31] R. Monthiller, A. Loisy, M. A. R. Koehl, B. Favier, and C. Eloy, Surfing on turbulence: A strategy for planktonic navigation, *Phys. Rev. Lett.* **129**, 064502 (2022).
- [32] M. Nasiri, H. Löwen, and B. Liebchen, Optimal active particle navigation meets machine learning, *Europhys. Lett.* **142**, 17001 (2023).
- [33] H. J. Kappen, Path integrals and symmetry breaking for optimal control theory, *J. Stat. Mech.: Theory Exp.* (2005) P11011.
- [34] J. Pinti, A. Celani, U. H. Thygesen, and P. Mariani, Optimal navigation and behavioural traits in oceanic migrations, *Theor. Ecol.* **13**, 583 (2020).
- [35] E. Zermelo, Über das Navigationsproblem bei ruhender oder veränderlicher Windverteilung, *Z. Angew. Math. Mech.* **11**, 114 (1931).
- [36] G. B. Jeffery, The motion of ellipsoidal particles immersed in a viscous fluid, *Proc. R. Soc. London A* **102**, 161 (1922).
- [37] T. J. Pedley and J. O. Kessler, Hydrodynamic phenomena in suspensions of swimming microorganisms, *Annu. Rev. Fluid Mech.* **24**, 313 (1992).
- [38] R. Rusconi, J. S. Guasto, and R. Stocker, Bacterial transport suppressed by fluid shear, *Nat. Phys.* **10**, 212 (2014).
- [39] G. Junot, N. Figueroa-Morales, T. Darnige, A. Lindner, R. Soto, H. Auradou, and E. Clément, Swimming bacteria in Poiseuille flow: The quest for active Bretherton-Jeffery trajectories, *Europhys. Lett.* **126**, 44003 (2019).

- [40] J. Słomka, U. Alcolombri, E. Secchi, R. Stocker, and V. I. Fernandez, Encounter rates between bacteria and small sinking particles, *New J. Phys.* **22**, 043016 (2020).
- [41] L. S. Pontryagin, *Mathematical Theory of Optimal Processes* (Routledge, London, 1987).
- [42] F. P. Bretherton, The motion of rigid particles in a shear flow at low Reynolds number, *J. Fluid Mech.* **14**, 284 (1962).
- [43] Y. C. Chang and H. J. Keh, Translation and rotation of slightly deformed colloidal spheres experiencing slip, *J. Colloid Interface Sci.* **330**, 201 (2009).
- [44] C.-M. Hu and R. Zwanzig, Rotational friction coefficients for spheroids with the slipping boundary condition, *J. Chem. Phys.* **60**, 4354 (1974).
- [45] R. Bellman, The theory of dynamic programming, *Bull. Amer. Math. Soc.* **60**, 503 (1954).
- [46] K. Gustavsson and B. Mehlig, Statistical models for spatial patterns of heavy particles in turbulence, *Adv. Phys.* **65**, 1 (2016).
- [47] S. A. Richards, H. P. Possingham, and J. Noye, Diel vertical migration: modelling light-mediated mechanisms, *J. Plankton Res.* **18**, 2199 (1996).
- [48] L. Biferale, F. Bonaccorso, M. Bucciotti, P. C. D. Leoni, and K. Gustavsson, Zermelo's problem: Optimal point-to-point navigation in 2D turbulent flows using reinforcement learning, *Chaos* **29**, 103138 (2019).
- [49] C. Calascibetta, L. Biferale, F. Borra, A. Celani, and M. Cencini, Optimal tracking strategies in a turbulent flow, *Commun. Phys.* **6**, 256 (2023).
- [50] H. L. Pécseli and J. K. Trulsen, Plankton's perception of signals in a turbulent environment, *Adv. Phys.: X* **1**, 20 (2016).
- [51] F.-G. Michalec, I. Fouxon, S. Souissi, and M. Holzner, Zooplankton can actively adjust their motility to turbulent flow, *Proc. Natl. Acad. Sci. USA* **114**, E11199 (2017).
- [52] J. Qiu, N. Mousavi, K. Gustavsson, C. Xu, B. Mehlig, and L. Zhao, Navigation of micro-swimmers in steady flow: the importance of symmetries, *J. Fluid Mech.* **932**, A10 (2022).
- [53] T. Kiørboe, *A Mechanistic Approach to Plankton Ecology* (Princeton University Press, Princeton, NJ, 2008).
- [54] A. E. Bryson and Y.-C. Ho, *Applied Optimal Control: Optimization, Estimation, and Control* (Routledge, New York, 2018).
- [55] M. Galassi *et al.*, *GNU Scientific Library Reference Manual*, 3rd ed. (Network Theory Ltd., 2009).
- [56] S. Colabrese, K. Gustavsson, A. Celani, and L. Biferale, Flow navigation by smart microswimmers via reinforcement learning, *Phys. Rev. Lett.* **118**, 158004 (2017).
- [57] S. Muiños-Landin, A. Fischer, V. Holubec, and F. Cichos, Reinforcement learning with artificial microswimmers, *Sci. Robot.* **6**, eabd9285 (2021).
- [58] M. Nasiri and B. Liebchen, Reinforcement learning of optimal active particle navigation, *New J. Phys.* **24**, 073042 (2022).
- [59] G. Goon, Gaussian fields, <https://garrettgoon.com/gaussian-fields> (2021).